Journal of Building Engineering 28 (2020) 101020

Contents lists available at ScienceDirect

Journal of Building Engineering

journal homepage: http://www.elsevier.com/locate/jobe

Daytime radiative cooling: To what extent it enhances office cooling system performance in comparison to night cooling in semi-arid climate?

Elvire Katramiz, Nesreen Ghaddar *, Kamel Ghali

Mechanical Engineering Department, American University of Beirut, P.O. Box 11-0236, Beirut, 1107-2020, Lebanon

ARTICLE INFO

Keywords:
Radiative cooling
Phase change material storage tank
Ventilated double layer window
Passive cooling system

ABSTRACT

This work investigates the performance of a novel passive cooling system for an office space in hot and dry climate. A daytime radiative cooling (RC) panel was coupled with a phase change material (PCM) storage tank system where the nocturnal radiative cooling power was used to regenerate the PCM during nighttime and the diurnal power during daytime was used to reduce the window temperature. To predict system operation, a mathematical model was developed integrating the hydronic RC panel model, water/PCM system heat exchange model, and ventilated window and space model.

The developed model was applied to a case study in Beqaa area of inland Lebanon. It was found that the use of diurnal RC panel power for window cooling reduced the storage system size by 12.3% in comparison to the case where only night RC panel was used. The window cooling reduced the radiation asymmetry in the office and resulted in cost savings of 10% when operated during the summer.

1. Introduction

In the past few decades, a considerable amount of research examined and reported useful application of nocturnal radiative panels in buildings for cooling purposes [1]. The cooling obtained from radiative cooling (RC) panels during **clear and dry nights** was stored in different types of storage tanks in order to be used during daytime under direct sunlight when the highest cooling demand occurs. Saitoh et al. [2] proposed an energy-efficient dwelling that utilized a sky radiative panel with a large storage tank to store the energy. Ezekwe [3] performed experimental studies to show the potential of a radiative cooling system combined with a thermal storage tank. The panels that were used to achieve nighttime cooling consisted of metallic radiators that were broadband emitters. Nevertheless, such panels were unable to achieve large sub-ambient cooling due to their strong absorption of incoming atmospheric radiation outside the transparency window of the atmosphere (8–13 μm) [4]. Subsequently, efforts have been made to improve the cooling capacity of the nocturnal radiative panels. In 1959 and for the first time, Head [5] proposed the use of selective infrared emitters that enhanced the radiative cooling effect. Hence, different designs of spectrally selective nighttime surfaces were theoretically studied and experimentally tested [6,7]. The latter discovery did not however eliminate the need of storage system in building cooling applications where cooling is needed during sunshine hours.

In recent years, developments on improving surface characteristics to achieve daytime radiative cooling took place. However, realizing radiative cooling during daytime is more challenging due to the incident solar radiation that is in a wavelength range below the atmospheric window. This required a special design of RC panels with high reflection of solar radiation while simultaneously having a high emissivity within the atmospheric window to produce daytime cooling. This was experimentally proven in 2013 by Rephaeli et al. [8] for the first time using a new structure for the radiative panel based on nanophotonics. Since then, many researchers focused on finding the most effective design of daytime radiative cooling by testing different nanostructured materials [9,10]. In a recent study, Hua et al. [11] theoretically showed that a photonic radiative cooler formed of double-layer nanoparticle-based coatings was able to achieve approximately 5 °C below ambient air temperature with a maximum cooling power of 40 W/m^2 under dry weather conditions. Nevertheless, the small cooling amount provided by diurnal radiative cooling limited the possible options of its usage in passive applications. Hence, daytime radiative cooling cannot be used as a primary cooling source for buildings but rather as a complementary application that would help reduce the building overall cooling load.

It is thus of great importance to evaluate to what extent would it be beneficial to integrate daytime radiative cooling in passive applications by studying its effect on the downsizing of the storage system needed for

* Corresponding author.
E-mail address: farah@aub.edu.lb (N. Ghaddar).

https://doi.org/10.1016/j.jobe.2019.101020
Received 26 July 2019; Received in revised form 23 October 2019; Accepted 24 October 2019
Available online 25 October 2019

Nomenclature

A	Area (m^2)
C_p	Specific heat (J/kg·K)
dt	Time step (s)
f	Melted fraction
F	View factor
h	Convective heat coefficient ($W/m^2.K$)
H	Tank height (m)
L	Tank length (m)
Lf	Latent heat of fusion of the PCM (kJ/kg)
L_{gap}	Air gap thickness (m)
m	Mass (kg)
$\dot{m}$	Mass flow rate (kg/s)
$Npcm$	Number of PCM spheres in each tank segment
PMV	Predicted Mean Value
PPD	Predicted Percentage dissatisfied
RC	Radiative cooling
RH	Relative humidity (%)
T	Temperature (°C)
Vss	Volume (m^3)

Greek Symbols

α	Absorptivity
ΔT_{pr}	Radiant temperature asymmetry (°C)
ε	Emissivity
ρ	Density (kg/m^3)
τ	Transmissivity

the building cooling due to the potential reduction in the daytime cooling load. Subsequently, the relatively small diurnal cooling power of the RC panel can be exploited in a daytime application aiming to lower the cooling load of a building space. One obvious possibility would be cooling a window in order to reduce its temperature. In fact, windows are typical components that can be target for cooling in **desert climates** where radiative panels are effective due to low humidity and clear skies [12]. During hot and arid summer time, the windows cause overheating which leads to an increase in the cooling load and provokes radiation asymmetry that affects the thermal comfort inside the space. This could be avoided by using the diurnal cooling power of the radiative panel as a supplementary load reduction method. The latter would help in reducing the heat gain to the space, which results in reducing the storage tank size. One promising thermal storage media to be combined with the radiative cooling system is Phase Change Material (PCM) [13,14]. These materials have the capability to store thermal energy at a relatively constant temperature [15], which benefits the system operation. The employment of the PCM in a water tank can provide the required thermal storage for daytime use via phase change: At night, the PCM would solidify and store enough cold energy that would be utilized during daytime for cooling purposes.

In this work, the impact of implementation of daytime radiative cooling on the storage system size is investigated through a case study for meeting thermal comfort and air quality needs of a typical office space in Beqaa Valley – Lebanon. The system consists of a hydronic RC panel for day/night time application combined with a PCM storage tank for daytime cooling purposes and a diurnally cooled glazed window. An integrated dynamic mathematical model of the proposed system is developed to examine the advantages of daytime RC and its impact on the storage system size compared to the case when only radiative night cooling is implemented. The interest resides in minimizing the system cost while maintaining indoor thermal comfort and air quality during daytime in hot and dry climate.

2. System description

A hybrid passive cooling system that combines the use of a water-based radiative cooling panel and a PCM thermal storage tank is proposed to meet the daytime cooling needs of an office space. Fig. 1 presents the proposed design of the integrated passive cooling systems for night and day operations. The hybrid water-based radiative cooling panel mounted on the office roof generates cool water that is used in the PCM storage tank for nocturnal thermal storage and in a water-air heat exchanger to cool down the window for diurnal space load reduction. During nighttime, the water flows in tubes embedded in the RC panel at (1) to cool down due to the radiative heat exchange between the panel and the outer space. At the exit of the panel (2), the cold water flows into a PCM storage tank that stores the cooling power generated by the RC

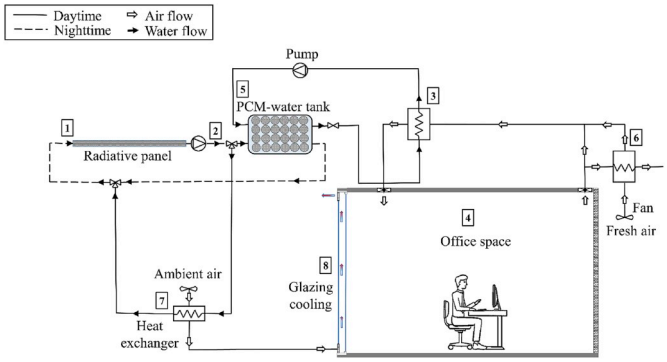

Fig. 1. Schematic of the hybrid system application.

panel. During daytime, the cooling energy of the water flowing through the PCM tank is released via a heat exchanger (3) to an airflow that is used to remove the heat load from the office space (4). The water constantly flows in a closed loop from the heat exchanger back to the PCM storage system where it loses its heat to the PCM. To ensure good air quality inside the space, a fresh airflow fraction of 8 l/s/person [16] is cooled using part of the return air (6) before being mixed with the rest of the exhaust air from the office. As for the RC panel, its daytime cooling power is harvested in cooling the window of the considered office. This technique consists of lowering the temperature of the air entering the ventilated double-layer window to reduce the heat gain to the space and minimize the asymmetric radiation that may occur. Thus, the cool water provided by the RC loses its cooling power via a heat exchanger (7) to the ambient air that flows into the double-layer window (8) to reduce its temperature.

2.1. Mathematical modeling

In order to study the performance of the proposed system, simplified component models were developed for each of the sub-systems; the hydronic radiative cooling system, the PCM storage tank and the office space models. The three models were integrated to simulate the operation of the system and predict the air temperature inside the office as well as the cooling power needed to maintain thermal comfort for occupants and good air quality in the office space during occupancy hours.

2.2. Radiative panel model

The model of the hydronic radiative cooler of Weimin et al. [17] was adopted. It predicts the water temperature through the pipes of the RC panel system shown in Fig. 2. It assumes 1-D transient flow in the pipes,

which leads to a unidirectional variation of the water temperature.

The panel is discretized into different sections along its length as presented in Fig. 2.a. Each segment assumes a constant surface temperature. The water temperature in segment *i* of the panel is governed by equation (1):

$$\rho_w V_i \; C_{p_w} \frac{dT_{w,RC(i)}}{dt} = \dot{m}_{w,RC} \; C_{p_w} (T_{w,RC}(t, \; i-1) - T_{w,RC}(t,i)) - \; Q_{net}(\mathrm{t,i}) \; A_i \tag{1}$$

and

$$Q_{net}(t,i) \; = Q_{rad}(t,i) - Q_{atm}(t) - Q_{sun}(t) - Q_c(t,i) \tag{2}$$

The left term of equation (1) represents the transient storage term, the first term to the right is the net convective heat flow and the last term is the net cooling power of the RC panel. $T_{w,RC}(t,i-1)$ and $T_{w,RC}(t,i)$ are respectively the inlet and outlet water temperature of segment *i* at time ??; V_i is the volume of the water in segment *i*, ρ_w and C_{p_w} are the density and the specific heat capacity of the water respectively, $\dot{m}_{w,RC}$ is the mass flowrate of the water in the segment and A_i is the area of the considered segment of the panel. $Q_{net}(\mathrm{t,i})$ is the time-dependent net cooling power per unit area of segment *i* of the radiative panel, and it is described by the energy balance in equation (2) that consists of the different heat transfer processes (see Fig. 2.b): the longwave radiative power emitted per unit area by the surface of segment *i* $Q_{rad}(t,i)$, which is dependent of the radiative surface temperature $T_S(t,i)$ (equation (3)); the absorbed power per unit area due to the incident atmospheric thermal radiation $Q_{atm}(t)$, which is dependent of the ambient atmosphere temperature $T_{ambient}$ (equation (4)); the absorbed power per unit area due to the incident solar radiation $Q_{sun}(t)$, which is minimized due to the use of the reflective upper layer that reflects solar radiation as previously stated (equation (5)); and the power lost/gained per unit area $Q_c(t,i)$ due to convection with the ambient air at the upper side of the panel and conduction through the roof to the inner space of the office.

$$Q_{rad}(t,i) \; = \; 2 \; \pi \; \int_0^{\frac{\pi}{2}} \sin\theta \cos\theta \; d\theta \; \int_0^{\infty} I_{BB}(T_S(t,i) \; , \; \lambda) \; \varepsilon(\lambda,\theta) \; d\lambda \tag{3}$$

$$Q_{atm}(t) = \; 2 \; \pi \; \int_0^{\frac{\pi}{2}} \sin\theta \cos\theta \; d\theta \; \int_0^{\infty} I_{BB}(T_{amb}(t), \; \lambda) \; \varepsilon(\lambda,\theta) \; \varepsilon_{atm}(\lambda, \; \theta) \; d\lambda \tag{4}$$

$$Q_{sun}(t) \; = q_{solar}(t) \; \alpha_{solar} \tag{5}$$

Where $I_{BB}(T,\lambda)$ is the blackbody spectral intensity [18], $\varepsilon(\lambda,\theta)$ and $\varepsilon_{atm}(\lambda,\theta)$ are the emissivity of the surface and atmosphere respectively, considered independent of the zenith angle θ. Note that $\varepsilon_{atm}(\lambda)$ depends on the RH and cloud coverage [19]. α_{solar} is the surface's solar absorptivity and $q_{solar}(t)$ is the solar radiation on a horizontal surface in (W/m^2). $T_S(t,i)$, which is the temperature of the radiator surface, is taken to be equal to the average temperature of water flowing across each segment [13].

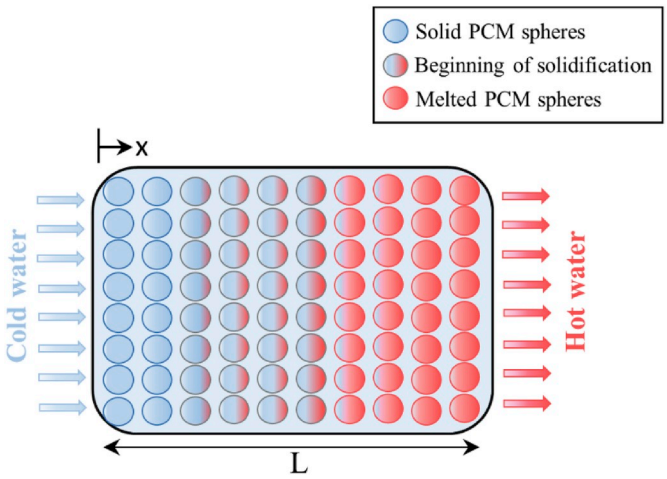

Fig. 3. Schematic of the PCM tank in the solidification phase during nighttime.

2.3. – PCM tank model

A horizontal storage tank (L » H) is filled with spherical capsules containing PCM (see Fig. 3) and assumed to be fully insulated. It is divided into *N* segments along its length, each of height equal to the spherical capsules diameter and containing the same number of PCM spheres [20]. The temperature of the water flowing through the tank is considered to vary longitudinally along the flow direction. The heat transfer in the volume of the sphere is neglected, therefore the PCM temperature is considered constant in the radial direction. A simplified mathematical model of the tank is adopted in this study [20] where the model is divided into two stages: i) the PCM single-phase thermal response in the sensible heat exchange stage and ii) the PCM melted fraction during the phase change stage.

2.3. *Sensible heat exchange with single phase PCM*

When the PCM does not experience any phase change ($T_{pcm} \neq T_{melting}$), its temperature is obtained by solving its enthalpy change equation due to the flow of water in the tank in the longitudinal direction *x*. The heat transfer between the PCM and water is mainly happening through convection since the PCM encapsulated shell is very thin and its material is highly conductive that the thermal resistance through it is negligible. Having the number of PCM spheres present (N_{pcm}) in each segment and the mass of each PCM sphere (m_{pcm}), the enthalpy change equation on each segment *k* of the storage tank is expressed as

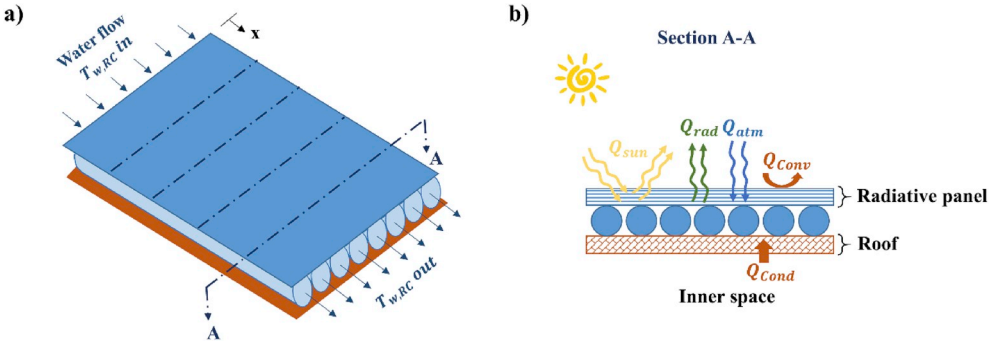

Fig. 2. a) Schematic of the RC panel and the water pipes; b) section of the rooftop radiative system.

$$m_{pcm}\ \ N_{pcm}C_{p_{pcm}}\frac{dT_{pcm_{(k)}}}{dt}=\left(T_{w,tank}(t,k)-\ \ T_{pcm}(t,k)\right)\ \ h_{pcm}\ \ \ A_{pcm} \tag{6}$$

Where the left side represents the transient storage term in the PCM and the right side constitute the convective heat flow between the PCM and the water. $C_{p_{pcm}}$ is the specific heat capacity of the PCM, $T_{w,tank}(t,k)$ and $T_{pcm}(t,k)$ are the temperatures of the water and the PCM in the tank segment k at time t respectively and A_{pcm} is the total PCM area in each segment. The convection heat transfer coefficient between the water and the PCM spheres, h_{pcm} is calculated using the correlation of forced convection in a sphere bed that has been introduced in Ref. [21].

The global conservation of energy for the water flow inside each segment of the tank is given by equation (7) and it includes the energy storage in the water (left side term), the net convective heat flow (first term of the right side) as well as the heat exchange between the water and the spherical capsules (second term of the right side).

$$\rho_w V_{sement}C_{p_w}\frac{dT_{w,tank_{(k)}}}{dt}=\ \ \dot{m}_{w,tank}\ \ \ C_{p_w}\ \ \left(T_{w,tank}(t,k-1)-\ \ T_{w,tank}(t,k)\right)-\ \ h_{w,pcm}\ \ A_{pcm}\ \ \left(T_{w,tank}(t,k)-T_{pcm}(t,k)\right) \tag{7}$$

Where $\dot{m}_{w,tank}$ is the water flowrate in the tank (kg/s).

2.3. Heat exchange during phase change

When the PCM in the tank attains the melting point, its temperature attains an almost constant value that is equal to the melting temperature ($T_{pcm}=T_{melting}$) and its melted fraction f is obtained by solving the following heat transport equation:

$$m_{pcm}L_f\frac{\partial f_{(k)}}{\partial t}=\left(T_{W,tank}(t,k)-T_{pcm}(t,k)\right)h_{pcm}A_{pcm} \tag{8}$$

where f is the liquid fraction of the PCM in segment k and L_f is the latent heat of fusion of the PCM. The term to the right side of the equation corresponds to convective heat transfer between the PCM and water in the considered segment.

2.4. Space model

The space model is important for the evaluation of the space-cooling load as well as the estimation of the indoor temperature and glazing temperature throughout the day. The space is divided into two main components as shown in Fig. 4: the double-layer window and the inner space of the office.

2.4. Glazing model

The following glazing model was implemented by Al Touma et al. [22] where it was experimentally validated. The glazing section consists of three main layers: the outer glass, the air gap and the inner glass (Fig. 4.a). Energy balance equations are carried out for each layer in order to get the surface temperatures of the inner glass ($T_{ig_{in}}, T_{ig_{out}}$) and outer glass ($T_{og_{in}}, T_{og_{out}}$) as well as the air gap temperature (T_a). Heat transfer processes in this double-layer glazed window consist of conduction in each glass layer, convection between each glass surface and its surrounding air and radiation between the glazing layers, radiation with the space internal envelope as well as with the outer space. During daytime, the solar radiation absorbed by the glazing is assumed to be uniformly distributed across them. Moreover, no energy storage is considered inside the glazing due to its small thickness. The energy balance equations at the external and internal boundaries of the outer glass are given respectively by

$$h_{Cout}\left(T_{amb}-T_{og_{out}}\right)+\alpha_{g_o}q_{sun}+h_{r,\ sky}\left(T_{sky}-T_{og_{out}}\right)+h_{r,\ ground}\left(T_{ground}-T_{og_{out}}\right)+\frac{k_{og}}{t_{og}}\left(T_{og_{in}}-T_{og_{out}}\right)=0 \tag{9}$$

$$\frac{K_{og}}{t_{og}}\left(T_{og_{out}}-T_{og_{in}}\right)+h_{r_{og-ig}}\ \left(T_{ig_{out}}-T_{og_{in}}\right)+h_{c_a}\left(T_a-T_{og_{in}}\right)=0a \tag{10}$$

For the inner glass, the energy equations at the external and internal boundaries are given respectively by

$$\frac{K_{ig}}{t_{ig}}\left(T_{ig_{in}}-T_{ig_{out}}\right)+h_{r_{og-ig}}\left(T_{og_{in}}-T_{ig_{out}}\right)+h_{c_a}\left(T_a-T_{ig_{out}}\right)+\tau_{g_o}\ \ \alpha_{g_i}\ \ q_{sun}=0 \tag{11}$$

$$\frac{K_{ig}}{t_{ig}}\left(T_{ig_{out}}-T_{ig_{in}}\right)+h_{cin}\left(T_{in}-T_{ig_{in}}\right)+q_{rad,\ in}=0 \tag{12}$$

where q_{sun} is the solar radiation on a vertical surface in (W/m^2), and $q_{rad,in}$ is the radiation heat exchange between the window and indoor space components including walls and ceiling. The radiation heat transfer coefficients $h_{r,ground}h_{r_{og-ig}}$, and $h_{r,\ sky}$ are given by Miyazaki et al. [23].

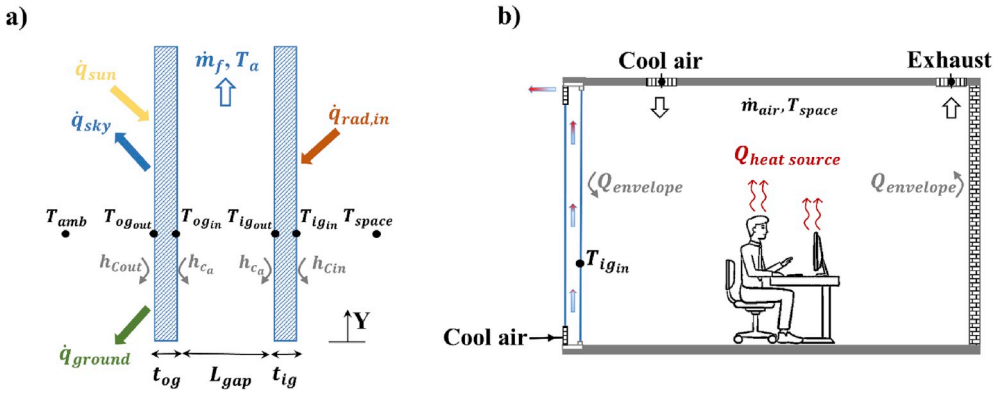

Fig. 4. Schematic of a) double-layer glazed window energy balance; b) the inner space energy balance.

The air gap layer is discretized into different segments along the window height in the *Y*-direction, each having a length of Δy. The airflow energy balance is then given by

$$\rho_{air} V_j {}^{C}p_{air} \frac{dT_{a_{(j)}}}{dt} = \dot{m}_f {}^{C}p_{air}\left(T_{a,j-1} - T_{a,j}\right) + h_{c_a}\left(T_{og_{in}} - T_{a,j}\right) \mathrm{W}_{\mathrm{glass}} \Delta \mathrm{y} + h_{c_a}\left(T_{ig_{out}} - T_{a,j}\right) \mathrm{W}_{\mathrm{glass}} \Delta \mathrm{y} \quad (13)$$

The left side of equation [14] represents the energy stored in the air; the right side includes the rate of increase in the energy of the air stream flowing through the control volume V_j and the convection between the air and the surrounding glass surfaces. The correlations for the convective heat coefficient h_{c_a} is extracted from ISO 15099 [24]:

$${}^{h}c_a = 2h_c + 4v_{air} \quad (14)$$

Where v_{air} represents the mean velocity of the air in the gap and h_c, the convective heat coefficient in a non-ventilated air gap which correlations are extensively detailed in Ref. [25].

2.5. Inner space model and thermal comfort

The global conservation of energy equation for the air in the space is defined as:

$$\rho_{air} V_{space} {}^{C}P_{air} \frac{dT_{space}}{dt} = \dot{m}_{air} {}^{C}P_{air}\left(T_{air_{in}} - T_{space}\right) + Q_{envelope}(\mathrm{t}) + Q_{heat\ source}(\mathrm{t}) \quad (16)$$

where the left term represents the transient storage in the air, the first term of the right side constitute the net convective heat flow, $Q_{envelope}(t)$ is the convective heat exchange between the indoor air and the space envelope and $Q_{heat\ source}(t)$ is the extra heat source from occupants and equipment (see Fig. 4.b). $T_{air_{in}}$ is the air temperature entering the space after being cooled by the water provided by the PCM tank and $\dot{m}_{air}$ is the mass flowrate of the supplied/exhausted air (kg/s). The space model of Yassine et al. [26] is adopted to solve for the walls' inner surface temperatures; each wall is considered to be a multi-layer wall and is discretized accordingly to predict the temperature distribution along these layers given the building envelope materials as well as the external ambient and internal conditions.

To define the occupants' thermal comfort in the office space which affects their performance and overall productivity, the ASHRAE 55 comfort model was used which is based on Fanger's Predicted Mean Vote (PMV) index [27]. The model requires the office air temperature and speed, the RH, the metabolic rate and clothing insulation of the occupants as well as the mean radiant temperature (MRT) which is calculated based on ASHRAE handbook [16]. Furthermore, the presence of the window leads to an asymmetrical radiative environment in the

Table 1
Time step independence testing using 4 different time steps.

	Time step (s)	Relative difference in space air temperature with previous case value (%)
Case 1	400	
Case 2	300	0.65
Case 3	200	0.53
Case 4	100	0.25

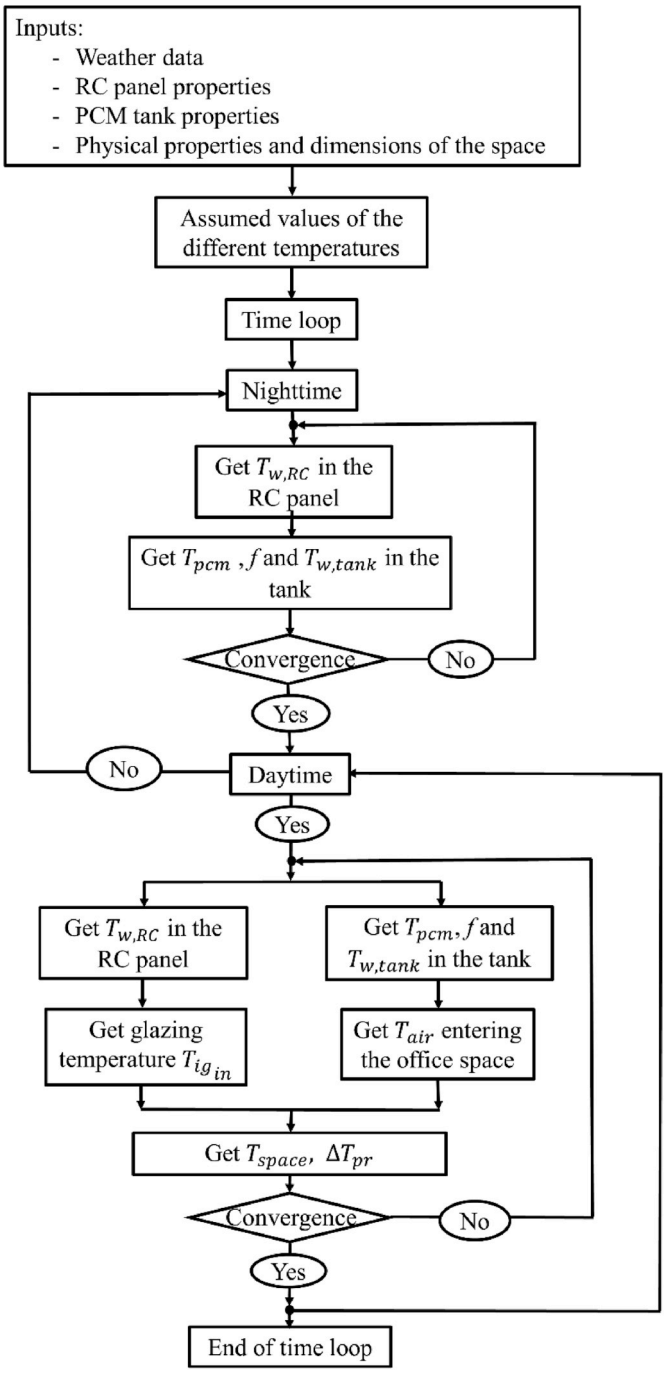

Fig. 5. Flow chart of the numerical modeling methodology.

office space where thermal comfort sensation may be sacrificed due to the exposure to high surface temperatures [22]. Subsequently, the radiant temperature asymmetry ΔT_{pr} can be a very critical factor in thermal comfort, especially in the case where occupants may be exposed to a highly non-uniform thermal radiation field. It is calculated for a person that is considered seated 1 m away from the window since the issue of asymmetry would be more critical the closer the person is to the source causing it [16,28].

2.6. Numerical methodology and control strategy

Simulations were carried out using a developed MATLAB code consisting of an implicit first-order time integration numerical scheme. The numerical model included the integration of the following sub-models: RC panel model, PCM/water tank model, ventilated double-layer glazing model and space model. Simulations were repeated over a number of cycle days until a steady periodic solution state was reached. The weather data, RC panel properties as well as the PCM characteristics were primary input used in the model. Input data for the dimensions and thermal properties of each system were also compiled for each sub-model. The solution was initialized at time $t = 0$ and an implicit scheme was employed which allowed the use of larger time steps leading to a shorter simulation runtime. Based on the time step independence test shown in Table 1, a time step of 100 s was used.

Fig. 5 summarizes the path followed to calculate the needed outputs from the developed model. During nighttime, and starting from the RC panel model that predicts the temperature of the water flowing through the panel, the temperature of the water entering the tank was computed. Then, solving the different equations of the PCM/water tank model, the temperature of the PCM spheres, their melted fraction as well as the temperature of the water inside each segment of the tank were obtained. During daytime, the glazing and space models were added. Hence, the RC panel model was coupled with an air/water heat exchanger to predict the temperature of the air entering the double layer window and the glazing model was used to determine the temperature of the glazing surface in contact with the inner space. On the other hand, the PCM/water tank model was coupled with a water/air heat exchanger to determine the temperature of the air brought to the space. Finally, the outputs of the daytime section were used as inputs to the space model in order to get the air temperature inside the office as well as the mean radiant temperature while taking into consideration the effect of all components.

The criterion for convergence was set when the difference between the new value of a parameter at time step t and its old value at the same time step is less than 10^{-5}. After convergence was attained at the current time step, the model advanced in time and solves for the next time step until the end of the simulation time. In order to preserve thermal comfort inside the office space, the flow rate of space supply air $\dot{m}_{air}$ was varied to maintain the air temperature in the office at 24 °C (±0.3 °C), providing thermal neutral conditions for the occupants.

2.7. Description of the case study

In order to assess the effectiveness of the proposed system in providing indoor thermal comfort while reducing the storage system size, two case studies were carried out of a typical office space (5 m × 5 m × 3 m) located in Beqaa Valley – Lebanon: i) A base case without window cooling referred to as case 1, and ii) a case study where the window cooling is implemented using the diurnal RC panel, noted as case 2. Beqaa is known for its semi-arid climate with hot and dry summers, a feature that is mandatory to fulfil the optimal performance of the radiative panel. Representative summer days were considered at the 15th of each month, June through September. The weather data presented in Table 2 was directly derived from hourly measured data files of the inland Lebanese climate [29].

Table 3
Office construction specifications [22,32,33].

Parameter	Properties
External south wall	15 cm concrete layer insulated with an 8 cm insulation layer - U = 0.76 W/m^{2}K
Ceiling	15 cm reinforced concrete layer with an 8 cm insulation layer - U = 0.77 W/m^{2}K
Internal walls	10 cm lightweight concrete
Window glazing	8 mm clear glass – air gap = 10 mm - $\alpha = 0.19$ - $\tau = 0.74$ - $\varepsilon = 0.84$ – k = 0.8 W/m.K

Table 2
Ambient temperature T_{amb} and solar radiation on a horizontal surface q_{solar} for the 15th of each summer month for the inland Lebanese climate.

	June		July		August		September	
Time	T_{AMB} (°C)	q_{solar} (W/M^2)	T_{AMB} (°C)	q_{solar} (W/M^2)	T_{AMB} (°C)	q_{solar} (W/M^2)	T_{AMB} (°C)	q_{solar}(W/M^2)
1:00 AM	14.41	0	23.7	0	18.3	0	17.9	0
2:00 a.m.	14.1	0	21	0	16.4	0	16.8	0
3:00 AM	13.7	0	18.7	0	16.4	0	14.8	0
4:00 AM	12.50	0	17.1	0	14.4	0	14.8	0
5:00 AM	12.10	0	15.6	0	13.7	0	13.7	0
6:00 AM	14.40	91.6	17	67.5	15.2	25.7	13.71	16.6
7:00 AM	18.70	240	21.3	216	16.8	171.4	13.3	123
8:00 AM	23.70	382.6	26.4	361.2	24.4	325.3	22.5	280.3
9:00 AM	26.00	667.5	28.7	643.5	28.7	459.9	28	418.8
10:00 AM	28.00	794.4	31.2	775.1	31.6	741.1	31.2	688.8
11:00 AM	30.40	909.6	33.6	900	34.1	871.7	33.2	810.6
12:00 PM	32.40	890.2	34.5	884.9	36.2	854.8	32.8	783.8
1:00 PM	33.20	877	34.5	862.5	35.3	832.9	34.1	759.1
2:00 PM	33.60	820	35.3	818.3	36.6	783.5	33.6	699.6
3:00 PM	34.10	706.7	34.9	704.7	36.2	662.4	32.8	430.4
4:00 PM	33.60	426.3	34.5	418.2	34.1	381.5	31.6	294.5
5:00 PM	32.00	200.2	33.2	161	29.9	118.2	28.3	118.2
6:00 PM	31.20	129.2	32	125.4	26.4	106	26.4	98.5
7:00 PM	29.50	0	28.7	0	24.8	0	24	0
8:00 PM	24.00	0	25.2	0	22.9	0	22.5	0
9:00 PM	22.10	0	24	0	22.1	0	21	0
10:00 PM	22.10	0	22.1	0	21	0	20.2	0
11:00 PM	19.80	0	20.2	0	20.2	0	20.2	0
12:00 AM	19.80	0	20.2	0	20.2	0	20.2	0

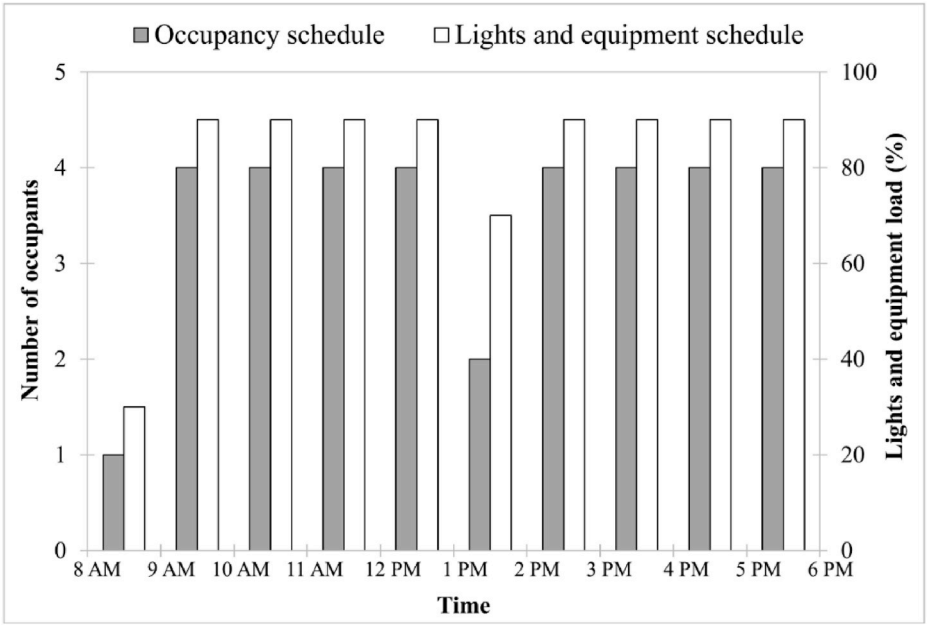

Fig. 6. Occupancy schedule and lights and equipment schedule inside the office space during office hours [30].

Table 4
RT18HC properties [35].

Thermo-physical properties	
Melting temperature T_m [°C]	18
Latent heat of fusion L_f [kJ/kg]	260
Specific heat capacity C_{pcm} [kJ/kg·K]	2
Density ρ_{pcm} [kg/m^3]	800

2.8. Space properties

In both considered cases, the same space characteristics were considered; the office was exposed to the outside from the window side only. A double layer window covered 60% of the south wall which is the only wall exposed to outside conditions. As for the ceiling, it was considered insulated to restrain any heat exchange with the RC panel. Further information concerning the space envelope is presented in Table 3. It was assumed that four people were present in the office during daytime. Each person generated 75 W while the load from equipment and lights was fixed at 16 W/m^2 [16]. A typical office occupancy schedule as well as lights and equipment schedule were extracted from ASHRAE 90.1–2004 [30] and presented in Fig. 6. The metabolic rate of the occupants and summer indoor clothing level were set at 1.2 and 0.5 respectively for a typical office space [31].

2.9. Storage system characteristics

The storage tank consists of Phase Change Material (PCM) placed inside highly conductive spherical capsules and placed in an insulated water-PCM storage tank. In fact, a sphere based packed bed storage system was reported to achieve more effective thermal performance compared to the other configurations [34]. During night, when the temperature of the water surrounding the PCM spheres drops due to nighttime radiative cooling, the spheres solidify as they release their energy to the water. During day, the temperature of the PCM spheres rises as they absorb heat, causing them to melt and liquefy. RT18HC paraffin was the PCM chosen for this application; it is commercially available by Rubitherm [35] with a melting temperature of 18 °C, and its thermo-physical properties are presented in Table 4. The cost of such PCM is $12.5/kg [35].

To obtain the needed PCM mass, the storage system cooling power should be able to remove the load of the office. Subsequently, the storage system should be sized based on the month with the peak conditions that necessitates the highest cooling load in comparison to the other considered months. Note that the cooling load changes in case 2 compared to case 1 due to the window load decrease when diurnal RC panel is used.

2.10. RC panel properties

The RC panel used in case 1 is a nocturnal RC panel consisting of an emissive layer; whereas the daytime RC panel was formed of the same

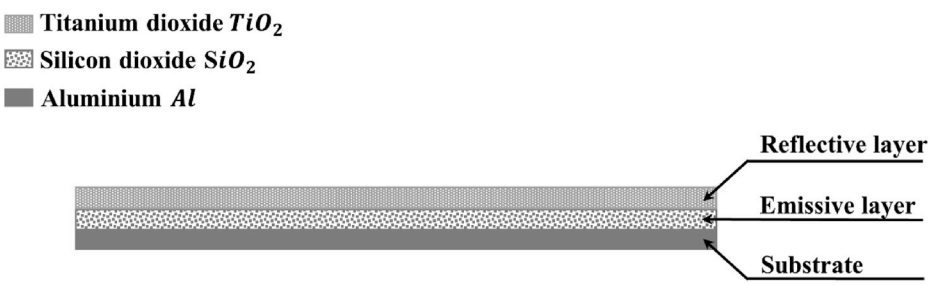

Fig. 7. RC panel materials and design.

emissive layer used in case 1 with the addition of the reflective layer. The diurnal radiative panel of the study of Hua et al. [11] was adopted in this work due to its scalable coating that has significant potential in large scale applications at a relatively low cost: It consisted of a double-layer coating composed of a reflective layer on top of an emissive layer, both lingering on an Al substrate (see Fig. 7). The reflective layer usage was primordial since reaching meaningful daytime radiative cooling would be highly dependent on preventing solar irradiation from being absorbed by the cooler. Titanium dioxide TiO_2 was chosen as a reflective material due to its high reflectivity in the solar spectrum (0.3–2.5 μm) and transparency in the mid to far infrared spectrum so that the thermal emission property of the double-layer coating is mainly dependent on the bottom emissive layer. The optimal thickness of the TiO_2 layer was reported to be 25 μm. As for the emissive layer components, Silicon dioxide SiO_2 and Silicon carbide SiC were reported to have strong optical emission in the sky window. In this study, SiO_2 is chosen to form the emissive layer for both the daytime and nighttime panels, with a 20 μm thickness. The optical properties of these layers were experimentally measured by Hua et al. [11]. The nighttime performance of the RC panel was the same for both considered cases since the reflective layer present in the daytime panel only affected the short wavelength range and thus, did not have any influence on the nighttime application. Hua et al. [11] reported that the radiative surface had a high emissivity (~ 0.9) in the sky window and a solar reflection of around 0.95. The cost of the nanoparticles applied in the manufacturing of the diurnal panel was reported to be $\$7/m^2$ [11].

The cooling power provided by the RC panel should be sufficient to regenerate the PCM mass used during night. Thus, the area of the RC panel should be fixed based on the required nocturnal cooling power and is evaluated through the simulations. The cloud coverage during the considered months was in the range of 0 and 0.12 and the RH varied between 20% and 56% [36]. Note that these two parameters have a fairly large effect on the spectral transmittance of the atmosphere, which in turn affects the cooling performance of the panel [19]. Subsequently, the emissivity of the atmosphere was calculated with the given air temperature, RH and the amount of cloud coverage using the correlations provided by Berger [19] and Argiriou et al. [37]. As for the rate of the water flowing through the RC panel system, it was fixed at 0.16 kg/s [13].

The proposed case studies were simulated using the developed model and the performance of the integrated system was extensively studied for the representative day of the months of June, July, August and September. The system was set to work from 8:00 a.m. until 6:00 p.m. which is the occupancy time of the office.

3. Results and discussion

The developed mathematical model in this study was an integration of previously validated and well-documented models in literature [11, 17,20,22,26]]. It was simulated for the two proposed case studies in order to evaluate and compare their performance for each considered month. Each case needs to maintain an air temperature of around 24 °C inside the office as a basis for comparison.

In the base case referred to as case 1, a nighttime RC panel is used to regenerate the PCM mass during night so that it provides the cooling energy needed to remove the space load during day. Preliminary simulations of the base case showed that a total PCM (RT18HC) mass of 114 kg can provide sufficient cooling energy to the office space during the peak conditions of the month of July. Subsequently, two identical horizontal PCM storage tanks were used, each having a size of 0.135 m^3 and containing 57 kg of PCM spheres of a diameter of 0.05 m each. Furthermore, in order to produce the cooling energy needed to regenerate this mass of PCM during nighttime, a RC panel area covering 60% of the roof ($5\times3\ m^2$) was used to provide cold water that is able to solidify the mass of PCM used.

In case 2, a diurnal RC panel is implemented to cool the office window during day while proving the regeneration of the PCM at night. This panel consists of adding a reflective layer to the nocturnal panel used in case 1 to reflect solar radiation and provide daytime cooling. The latter will reduce the radiant asymmetry from the window and the load of the office space due to the reduction in the window load. Accordingly, the PCM mass needed to remove the space load will decrease. Therefore, simulations of this case were performed in order to study the effect of the daytime radiative cooling implementation on the office load and possible PCM mass reduction along the associated cost reduction as well as the radiant asymmetry in the office.

3.1. Base case without window cooling

The simulation of the proposed system was first achieved for the base case where there is no window cooling. For each summer month, the supplied air mass flowrate $\dot{m}_{air}$ should maintain an indoor air temperature of around 24 °C throughout the day. Subsequently, it changed on an hourly basis depending on the inner space load and outdoor conditions, as presented in Table 5. During early morning operation in the month of July (8:00 a.m.–9:00 a.m.), a low value of 0.08 kg/s of air flowrate was needed since the outdoor temperature, solar radiation intensity as well as the inner space load (occupants, lights and equipment) were low. As these quantities increased, higher air flow rates were required in order to meet the office cooling load. It was found that from 12:00 p.m. to 1:00 p.m. where peak cooling load is to be removed, a maximum value of 0.195 kg/s was needed. On the other hand, between 1:00 p.m. and 2:00 p.m., a reduction in the required mass flow rate was noticed ($\dot{m}_{air}$ = 0.15 kg/s). This was caused by the typical office break during this period (see Fig. 6), which led to a decrease in inner space load. After the end of the break period, $\dot{m}_{air}$ increases to 0.18 kg/s. From 3:00 p.m. till the rest of the day, the needed flowrate decreases again as the outdoor conditions and solar intensity drop. The same trend of flowrate hourly variation was found during each month; however, the values differed with respect to the outdoor weather conditions and solar intensities.

As previously stated, the air temperature inside the office space was maintained at 24 °C (±0.3 °C) during office hours for all the considered months since it is known to provide thermal comfort in typical office environments. In fact, a Predicted Mean Vote (PMV) between 0.02 and 0.3 with a Predicted Percentage dissatisfied (PPD) ranging between 5 and 7% were found for the considered months. Thus, the overall comfort achieved in the office was acceptable since the PMV and PPD were in the limits of thermal comfort defined by ASHRAE ($|\ PMV\ | < 0.5$ and $PPD < 10\%$). Nevertheless, the presence of the window leads to an asymmetrical radiative environment in the office; Table 6 presents the hourly averaged radiant temperature asymmetry of a person seated 1 m away from the window as well as the temperature of the glazing surface that is subjected to the inner space conditions for all the considered months. In the month of July, a radiant temperature asymmetry ΔT_{pr} of 8.12°C was found during the first working hour and increased to reach a peak value of 12.35 °C at peak conditions (between 12:00 p.m. and 1:00 p.m.), inducing local dissatisfaction to the occupant. The noted radiant temperature asymmetry was caused by the high temperature of the

Table 5
Hourly averaged mass flowrate of the supplied air $\dot{m}_{air}$ (kg/s) in the base case.

Time	June	July	August	September
*8:*00 a.m. - *9:*00 a.m.	0.07	0.08	0.065	0.06
*9:*00 a.m. - *10:*00 a.m.	0.17	0.175	0.175	0.175
*10:*00 a.m. - *11:*00 a.m.	0.185	0.185	0.185	0.185
*11:*00 a.m. - *12:00 p.m.*	0.19	0.19	0.192	0.19
12:00 p.m. - 1:00 p.m.	0.195	0.195	0.198	0.195
1:00 p.m. - 2:00 p.m.	0.15	0.15	0.155	0.15
2:00 p.m. - 3:00 p.m.	0.18	0.18	0.185	0.18
3:00 p.m. - 4:00 p.m.	0.17	0.17	0.17	0.165
4:00 p.m. - 5:00 p.m.	0.155	0.155	0.15	0.148
5:00 p.m. - 6:00 p.m.	0.14	0.14	0.13	0.13

Table 6
Hourly averaged radiant temperature asymmetry ΔT_{pr} and temperature of the glazing inner surface $T_{ig_{in}}$ (°C) in the base case.

	June		July		August		September	
Time	ΔT_{pr}	$T_{ig_{in}}$	ΔT_{pr}	$T_{ig_{in}}$	ΔT_{pr}	$T_{ig_{in}}$	ΔT_{pr}	$T_{ig_{in}}$
*8:*00 a.m. - *9:*00 a.m.	7.90	33.27	8.12	33.86	7.64	32.80	7.02	31.61
*9:*00 a.m. - *10:*00 a.m.	9.51	36.08	9.77	36.45	9.94	36.40	9.35	35.82
*10:*00 a.m. - *11:*00 a.m.	10.82	37.71	11.28	38.43	11.45	38.55	11.00	38.01
*11:*00 a.m. - *12:00 p.m.*	11.66	38.90	12.17	39.78	12.33	39.82	11.80	39.14
12:00 p.m. - 1:00 p.m.	11.92	39.26	12.35	40.02	12.54	40.22	11.54	38.69
1:00 p.m. - 2:00 p.m.	11.36	38.74	11.58	39.04	11.62	39.07	11.02	38.10
2:00 p.m. - 3:00 p.m.	10.30	37.38	10.62	37.80	10.63	37.88	9.62	36.22
3:00 p.m. - 4:00 p.m.	8.84	35.51	8.97	35.64	8.78	35.68	7.65	33.67
4:00 p.m. - 5:00 p.m.	6.84	33.01	6.94	33.07	6.13	32.44	5.21	30.50
5:00 p.m. - 6:00 p.m.	4.34	29.79	4.44	29.87	3.15	28.09	3.16	27.84

Table 7
Hourly averaged radiant temperature asymmetry ΔT_{pr} and temperature of the glazing inner surface $T_{ig_{in}}$ (°C) in case 2.

	June		July		August		September	
Time	ΔT_{pr}	$T_{ig_{in}}$	ΔT_{pr}	$T_{ig_{in}}$	ΔT_{pr}	$T_{ig_{in}}$	ΔT_{pr}	$T_{ig_{in}}$
*8:*00 a.m. - *9:*00 a.m.	1.77	25.33	2.47	26.73	1.98	24.83	1.35	23.68
*9:*00 a.m. - *10:*00 a.m.	4.14	29.27	4.85	30.38	4.69	29.66	3.82	28.91
*10:*00 a.m. - *11:*00 a.m.	6.21	31.91	7.00	33.07	7.00	32.73	6.32	32.04
*11:*00 a.m. - *12:00 p.m.*	7.74	33.78	8.53	35.03	8.56	34.88	7.88	34.09
12:00 p.m. - 1:00 p.m.	8.43	34.91	9.17	35.95	9.21	36.10	8.15	34.44
1:00 p.m. - 2:00 p.m.	8.31	34.69	9.12	35.76	9.14	35.85	8.13	34.41
2:00 p.m. - 3:00 p.m.	8.09	34.34	8.56	35.08	8.58	35.24	7.47	33.50
3:00 p.m. - 4:00 p.m.	7.09	33.01	7.38	33.47	7.30	33.58	5.96	31.58
4:00 p.m. - 5:00 p.m.	5.55	30.99	5.75	31.32	5.16	30.95	3.96	28.90
5:00 p.m. - 6:00 p.m.	3.43	28.27	3.59	28.57	2.42	27.22	2.04	26.38

glazing surface $T_{ig_{in}}$ that increased from 33.86°C in the morning to 40.02°C at peak conditions and then dropped to around 30 °Cat the end of the day. This variation followed the same trend as that of the solar radiation intensity and weather conditions during the day. The same happened in the months of June, August and September, where a radiant temperature asymmetry peak of 11.92°C, 12.54 and 11.54 °C were respectively obtained.

Note that the initial PCM mass adopted at the beginning of the simulations (114 kg) was found to be enough to remove the space load in the different months: A total melted fraction of 95% was found at the end of the representative day of July, 93.1% in June, followed by a 92.7% total melting at the end of the day in August and finally reaching its minimum value in September with a 91.45% total melted fraction. Moreover, this PCM mass was successfully regenerated at the end of the night (around 4:00 a.m.) by the RC panel area that covered 60% of the roof.

3.2. Case study with window cooling implementation

In this case, a diurnal RC panel was implemented in order to harvest its daytime cooling power in reducing the high radiation asymmetry and glazing temperature obtained in the base case by cooling the window, leading to a reduction in the space load and storage system size while establishing local comfort for the occupants. Subsequently, a reflective layer of TiO_2 was added to the nocturnal RC panel of case 1, covering 60% of the roof. The cold water provided by this panel during sunshine hours helped in cooling an airflow of 0.07 kg/s that was supplied into the window gap to reduce the glazing temperature as well as the radiant

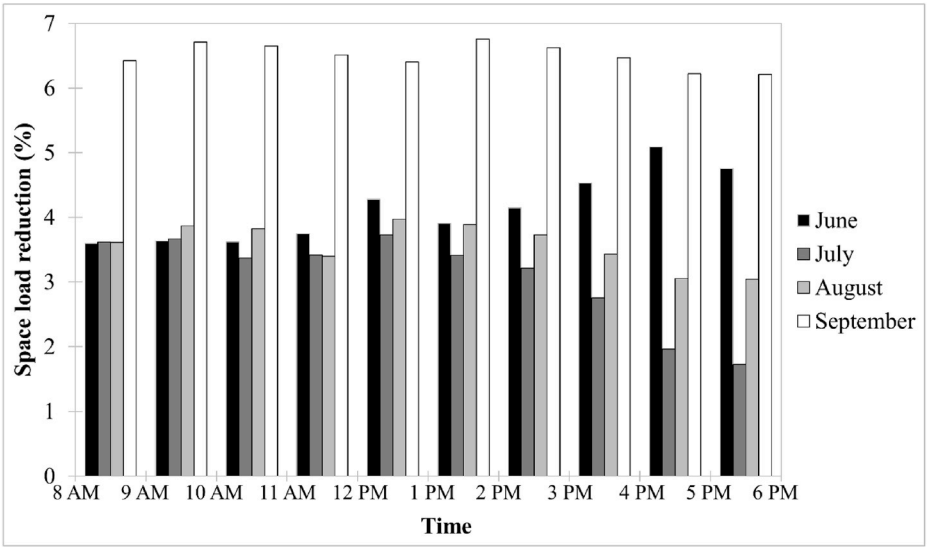

Fig. 8. Hourly averaged load reduction of case 2 in reference to the base case (%).

asymmetry in the space.

The hourly averaged radiant temperature asymmetry ΔT_{pr} and glazing inner surface temperature $T_{ig_{in}}$ are presented in Table 7 for each considered month. It can be observed that upon integrating the window cooling application to the system, the ΔT_{pr} value in the month of July is 2.47 °C between 8:00 a.m. and 9:00 a.m. It increased between 11:00 a.m. and 1:00 p.m. from 8.53°C to a peak of 9.17 °C. Lower ΔT_{pr} values were reached in the month of June and September throughout the day due to their moderate weather conditions and solar radiation intensities in comparison to those of July and August. This is explained by the fact that the RC panel performance during daytime enhances as the outdoor weather conditions and solar radiation intensity drop. Regarding the glazing inner surface temperature, a $T_{ig_{in}}$of 26.73°C was noted in the early morning of July. It increased to reach a value of 35.95°C between 12:00 p.m. and 1:00 p.m., and then decreased as the solar radiation intensity drops (1:00 p.m.–6:00 p.m.). The same trend of hourly glazing temperature variation is found in the other months as well. Comparing the ΔT_{pr} values of this case to those obtained in the base case (Table 6), a reduction of 29.2%, 25.7%, 26.55% and 29.4% during June, July, August and September was found respectively during peak conditions. This reduction is attributed to the reduction in the glazing inner surface temperature, which is noted to reach 11.08% in June, 10.16% in July, 10.24% in August and 11.24% in September at peak conditions.

The glazing temperature reduction obtained due to the window cooling also induced a decrease in the window load transmitted towards the inside of the office, as an average window load reduction of 35.6%, 34.05%, 31.16% and 29.9% was noted respectively in September, June, August and July. This window load reduction helped in reducing the space overall load. Fig. 8 shows the percentage of the space load reduction in case 2 in comparison to the base case. In each considered month, the load reduction changed throughout the day depending on the variation of weather conditions, solar radiation as well as window load. The average space load reduction during the office hours is 6.5% in September, 4.13% in June, 3.58% in August and 3.09% in July. It is subsequently found that the highest load reduction was reached during September due to its moderate diurnal weather conditions that enhanced the performance of the RC panel, followed by June, August and July where the peak conditions gave minimum load reduction.

This load reduction led to a decrease in the needed air mass flowrate to be supplied into the room; Table 8 shows the mass flowrate of the supplied air $\dot{m}_{air}$ in the case of window cooling. During the month of July, a rate of 0.04 kg/s is needed between 8:00 a.m. and 9:00 a.m. in comparison to 0.08 kg/s in the base case where no window cooling was applied (Table 5). This rate increases and reaches a maximum value of 0.17 kg/s during peak hour, which is 12.8% lower than the maximum airflow rate needed in the base case at peak conditions. Note that the hourly basis variation of $\dot{m}_{air}$ in this case follows the same trend as in the base case. It is also worth mentioning that the highest overall mass flow rate reduction is found during September, the month with the highest load reduction.

As the cooling load of the office experienced a drop when the window was cooled, a storage system size reduction was achieved: the PCM mass needed to meet the cooling load of the office was lower by 14 kg than the mass used in the base case. Subsequently, a total PCM mass of 100 kg was equally divided into the two tanks, each having a volume of 0.122 m^3. This 12.3% reduction in the PCM mass when cooling the window affects the overall cost of the system. Therefore, a cost analysis of the system is conducted.

4. System savings analysis

In order to be able to critically assess the proposed system's added value, a simple cost analysis was performed and each component cost was estimated separately. The diurnal RC panel used in case 2 was more expensive than the nighttime one used in case 1 due to the presence of the extra reflective layer that was estimated to cost about \$1.5/m^2. Subsequently, the nighttime RC panel price was \$5.5/m^2 whereas that of the daytime panel was \$7/m^2. Regarding the storage tank used, 114 kg of PCM were used in case 1 to meet the cooling load of the office and a total of 14 kg was reduced in case 2 due to the use of the diurnal RC panel. With a PCM cost of \$12.5/kg [35], a total PCM cost of \$1250 was hence needed in case 2 in contrast to a \$1425 in the base case.

Table 8
Hourly averaged mass flowrate of the supplied air $\dot{m}_{air}$ (kg/s) in case 2.

Time	June	July	August	September
8:00 a.m. - *9*:00 a.m.	0.025	0.04	0.03	0.018
9:00 a.m. - *10*:00 a.m.	0.13	0.135	0.135	0.132
10:00 a.m. - *11*:00 a.m.	0.15	0.155	0.155	0.153
11:00 a.m. - *12:00 p.m.*	0.165	0.165	0.165	0.162
12:00 p.m. - 1:00 p.m.	0.17	0.17	0.17	0.166
1:00 p.m. - 2:00 p.m.	0.135	0.135	0.135	0.132
2:00 p.m. - 3:00 p.m.	0.165	0.165	0.165	0.16
3:00 p.m. - 4:00 p.m.	0.16	0.16	0.16	0.148
4:00 p.m. - 5:00 p.m.	0.15	0.15	0.143	0.137
5:00 p.m. - 6:00 p.m.	0.13	0.135	0.125	0.125

The cost of the system for the considered summer months was computed as follows:

$$Cost \quad (\$) = I + \quad E_{elec} \times r \tag{17}$$

where I is the initial cost of the system (\$), E_{elec} is the electricity consumption for the considered summer months (KWh) and r is the electricity tariff rate in Lebanon (\$/KWh). The average tariff rate of electricity in Lebanon is currently of \$0.13/kWh [38]. The fan and pump power consumption were also calculated for both cases while considering: a) the extra pump and fan electric consumption during daytime for the window cooling in case 2 and b) the decrease in the power of the fan supplying the air to the office in case 2, which is due to the reduction in the mass flowrate found in comparison to the base case. This led to a comparable operation cost between the two cases, making the savings mainly affected by the initial cost. It was then found that the overall cost of the system of case 2 for the summer months was reduced by about \$152 from the base case. Thus, the resultant total savings of the diurnal RC panel integration were around 10% compared to the base case of typical night radiative cooling.

5. Conclusion

This paper evaluated the integration of daytime radiative cooling to a passive system and assessed its impact on the system size and overall cost. Two cases were extensively studied and compared: one including a system that used diurnal RC for daytime load reduction and another that used typical nighttime RC. A set of simulations was conducted based on a typical office space located in Beqaa Valley in Lebanon for the months of June, July, August and September. It was found that using daytime radiative cooling for window load reduction decreased the needed PCM mass by 14 kg. Accordingly, 10% savings in the overall system cost were attained, even though a higher initial cost for the daytime RC was needed. In addition, the proposed system resulted with better comfort conditions due to reduced radiant asymmetry as well as a smaller storage system at no added cost.

Although current work considered the daytime RC application in window cooling to reduce space load and window radiation asymmetry, however, there are other potential passive cooling applications for improving building performance in hot climates. One potential application for future studies is the use of RC captured power in pre-cooling ventilation fresh air to reduce air-conditioning cost. Other applications for diurnal RC may include condenser cooling to improve vapor compression system coefficient of performance by lower the temperature of air cooling the condenser. This indicates the need in future work to properly consider utilizing daytime RC by incorporating it in new

passive designs or as complementary design to existing cooling system to improve building energy performance.

Acknowledgment

The authors would like to acknowledge the financial support of the University Research Board of the American University of Beirut grant award. In addition, the American University of Beirut PhD scholarship to Ms. Katramiz is highly acknowledged.

References

[1] G. Mihalakakou, A. Ferrante, J.O. Lewis, The cooling potential of a metallic nocturnal radiator, Energy Build. 28 (3) (1998) 251–256, 11/01/1998.
[2] T.S. Saitoh, T. Fujino, Advanced energy-efficient house (HARBEMAN house) with solar thermal, photovoltaic, and sky radiation energies (experimental results), Sol. Energy 70 (1) (2001) 63–77, 01/01/2001.
[3] C.I. Ezekwe, Performance of a heat pipe assisted night sky radiative cooler, Energy Convers. Manag. 30 (4) (1990) 403–408, 01/01/1990.
[4] C. Granqvist, A. Hjortsberg, Surfaces for radiative cooling: Silicon monoxide films on aluminum, Appl. Phys. Lett. 36 (2) (1980) 139–141.
[5] A. Head, Method and Means for Refrigeration by Selective Radiation, 1959. Australian Patent, no. 239364.
[6] A. Gentle, G. Smith, Radiative heat pumping from the earth using surface phonon resonant nanoparticles, Nano Lett. 10 (2) (2010) 373–379, 02/10 2010.
[7] B. Orel, M.K. Gunde, A. Krainer, Radiative cooling efficiency of white pigmented paints, Sol. Energy 50 (6) (1993) 477–482, 06/01/1993.
[8] E. Rephaeli, A. Raman, S. Fan, Ultrabroadband photonic structures to achieve high-performance daytime radiative cooling, Nano Lett. 13 (4) (2013) 1457–1461, 04/10 2013.
[9] Y. Fu, J. Yang, Y.S. Su, W. Du, Y.G. Ma, Daytime passive radiative cooler using porous alumina, Sol. Energy Mater. Sol. Cells 191 (2019) 50–54, 03/01/2019.
[10] Z. Huang, X. Ruan, Nanoparticle embedded double-layer coating for daytime radiative cooling, Int. J. Heat Mass Transf. 104 (2017) 890–896, 01/01/2017.
[11] B. Hua, Y. Chen, W. Boxiang, F. Xing, C.Y. zhao, R. Xiulin, Double-layer nanoparticle-based coatings for efficient terrestrial radiative cooling. Solar Energy Materials and Solar Cells, 2017.
[12] X. Lu, P. Xu, H. Wang, T. Yang, J. Hou, Cooling potential and applications prospects of passive radiative cooling in buildings: the current state-of-the-art, Renew. Sustain. Energy Rev. 65 (2016) 1079–1097, 11/01/2016.
[13] S. Zhang, J. Niu, Cooling performance of nocturnal radiative cooling combined with microencapsulated phase change material (MPCM) slurry storage, Energy Build. 54 (2012) 122–130, 11/01/2012.
[14] M. Fiorentini, P. Cooper, Z. Ma, Development and optimization of an innovative HVAC system with integrated PVT and PCM thermal storage for a net-zero energy retrofitted house, Energy Build. 94 (2015) 21–32, 05/01/2015.
[15] R. Baetens, B.P. Jelle, A. Gustavsen, Phase change materials for building applications: a state-of-the-art review, Energy Build. 42 (9) (2010) 1361–1368, 09/01/2010.
[16] ASHRAE Handbook, "American Society of Heating, Refrigerating, Air-Conditioning, Engineers 2017 ASHRAE Handbook, 2017 (in English).
[17] N.F. Weimin Wang, Srinivas Katipamula, Modeling and Simulation of a Photonic Radiative Cooling System, 2016.
[18] J.A. Duffie, W.A. Beckman, Solar Engineering of Thermal Processes/John A. Duffie, William A. Beckman, Wiley, New York, 1991. https://nla.gov.au/nla.cat-vn615844.
[19] X. Berger, A simple model for computing the spectral radiance of clear skies, Sol. Energy 40 (4) (1988) 321–333, 01/01/1988.
[20] K.A.R. Ismail, J.R. Henríquez, Numerical and experimental study of spherical capsules packed bed latent heat storage system, Appl. Therm. Eng. 22 (15) (2002) 1705–1716, 10/01/2002.
[21] E. Achenbach, Heat and flow characteristics of packed beds, Exp. Therm. Fluid Sci. 10 (1) (1995) 17–27, 01/01/1995.
[22] A. Al Touma, K. Ghali, N. Ghaddar, N. Ismail, Solar chimney integrated with passive evaporative cooler applied on glazing surfaces, Energy 115 (2016) 169–179, 11/15/2016.
[23] T. Miyazaki, A. Akisawa, I. Nikai, The cooling performance of a building integrated evaporative cooling system driven by solar energy, Energy Build. 43 (9) (2011) 2211–2218, 09/01/2011.
[24] ISO, Thermal Performance of Windows, Doors and Shading Devices: Detailed Calculations," ISO 15099 Ed: International Organization for Standardization, ISO 15099, 2003.
[25] J.S. Carlos, H. Corvacho, P.D. Silva, J.P. Castro-Gomes, Modelling and simulation of a ventilated double window, Appl. Therm. Eng. 31 (1) (2011) 93–102, 01/01/2011.
[26] B. Yassine, K. Ghali, N. Ghaddar, I. Srour, G. Chehab, A numerical modeling approach to evaluate energy-efficient mechanical ventilation strategies, Energy Build. 55 (2012) 618–630, 12/01/2012.
[27] ASHRAE Standard 55, ASHRAE standard 55 thermal environmental conditions for human occupancy, Available: http://comfort.cbe.berkeley.edu/.
[28] N. Ghaddar, M. Salam, K. Ghali, Steady thermal comfort by radiant heat transfer: the impact of the heater position, Heat Transf. Eng. 27 (7) (2006) 29–40, 08/01 2006.
[29] M. Badawiyeh, N. Ghaddar, K. Ghali, Case study of trombe wall inducing natural ventilation through cooled basement air to meet space cooling needs, J. Energy Eng. 143 (2) (2016), 04016039.
[30] ASHRAE, ASHRAE 90.1 - Appendix G. Building Performance Rating Method, 2004.
[31] C. Ekici, A Review of Thermal Comfort and Method of Using Fanger's PMV Equation, 2013, pp. 61–64.
[32] Guardian glass., Available: https://www.guardianglass.com/us/en.
[33] Thermal Standard for Buildings in Lebanon, 2005.
[34] S. Aziz, N. Amin, M. Abdul Majid, M. Belusko, F. Bruno, CFD simulation of a TES tank comprising a PCM encapsulated in sphere with heat transfer enhancement, Appl. Therm. Eng. 143 (2018) 1085–1092, 10/01/2018.
[35] Rubitherm Rubitherm, Phase change material, Available: https://www.rubitherm.eu/en/index.php/productcategory/organische-pcm-rt.
[36] Weather forcast, Available: https://www.yr.no/place/Lebanon/.
[37] A. Argiriou, M. Santamouris, C. Balaras, S. Jeter, Potential of radiative cooling in Southern Europe, Int. J. Sol. Energy 13 (3) (1992) 189–203, 01/01 1992.
[38] T. Itani, N. Ghaddar, K. Ghali, Strategies for reducing energy consumption in existing office buildings, Int. J. Sustain. Energy 32 (4) (2013) 259–275, 08/01 2013.